INTERNATIONAL JOURNAL FOR NUMERICAL METHODS IN FLUIDS
Int. J. Numer. Meth. Fluids 2001; **35**: 357–370

Sensitivity of mesh spacing on simulating macrosegregation during directional solidification of a superalloy

P. K. Sung[a], D. R. Poirier[a,*,1] and S. D. Felicelli[b]

[a] *Department of Materials Science and Engineering, The University of Arizona, Tucson, AZ, U.S.A.*
[b] *Centro Atómico Bariloche, 8400 S. C. de Bariloche, Argentina*

SUMMARY

The sensitivity of mesh spacing on simulations of macrosegregation, particularly 'freckles', during vertical directional solidification of a superalloy in a rectangular mold was systematically analyzed to achieve accurate predictions in finite element calculations. It was observed that a coarser mesh spacing in the x-direction horizontal tends to minimize the simulated macrosegregation, whereas a coarser mesh spacing in the y-direction vertical artificially tends to make the system appear to have more macrosegregation. When solidification conditions either lead to a well-established freckling case or to a well-established non-freckling case, the simulated results are not sensitive to the mesh spacing provided the elements are no larger than about $2d_1$ by $2\,D/V$ and $3d_1$ by $4\,D/V$ respectively, where d_1 is the primary dendrite arm spacing, D is the diffusivity of the alloy solute with the smallest diffusivity in the liquid, and V is the growth rate. However, when solidification conditions are very close to the transition between freckling and no freckling, the simulated results are sensitive to the mesh spacing, especially in the y-direction. Based on the mesh sensitivity analysis from the two-dimensional simulations of rectangular castings of René N5, the mesh with element dimensions no larger than $2d_1$ in the x-direction and $1.5\,D/V$ in the y-direction are recommended as the most stringent element size. Copyright © 2001 John Wiley & Sons, Ltd.

KEY WORDS: dendritic single crystal; directional solidification; freckles; macrosegregation; mesh spacing

1. INTRODUCTION

Ni-based superalloys are used in critical components in gas-turbine engines because they exhibit outstanding creep resistance at elevated temperatures; moreover, the creep resistance of these alloys is further improved by controlling the grain structures. Specifically, directionally solidified (DS) and dendritic single-crystal (SC) castings represent the current casting

* Correspondence to: Department of Materials Science and Engineering, The University of Arizona, Tucson, AZ 85721-0012, U.S.A. Tel.: +1 520 6216072; fax: +1 520 6218059.
[1] E-mail: poirierd@u.arizona.edu

Received 3 January 2000
Revised 30 March 2000

technology, with the SC-castings being more creep resistant [1]. During solidification of both DS- and SC-castings, however, thermosolutal convection can cause a severe form of macrosegregation, known as 'freckles'. Freckles are observed as long and narrow trails, aligned roughly parallel to the direction of gravity in both DS- and SC-castings and are enriched in the normally segregating elements and depleted in the inversely segregating elements [2]. It is known that freckles are a direct consequence of upward-flowing liquid plumes that emanate from channels within the solid plus liquid region (called the 'mushy zone') during solidification [3]. In terms of transport phenomena, the channels are a manifestation of thermosolutal convection in a porous medium subject to remelting by interdendritic liquid. The formation of channels and freckles occurs when the fluid flow in the growth direction exceeds the isotherm velocity [4], particularly in the upper portion of the mushy zone where the fraction of solid is low.

When freckles are found in DS- and SC-castings, they are cause enough to scrap the expensive castings. Hence, it is important to predict this type of segregation and to develop suitable casting conditions to avoid the defects. The cooling of DS- and SC-castings is effected from below, so the temperature profile is gravitationally stable, but convection may still develop. In a binary alloy, when the solute alloy element is lighter than the solvent and is partitioned to the liquid during solidification, then the liquid is convectively unstable. In a multicomponent alloy, each alloying element contributes to a change in the density of the liquid. Some components decrease the density of the liquid while others increase it, depending on their respective solutal expansion coefficients.

The prediction of macrosegregation in multicomponent alloys dates to 1970, when Fujii *et al*. [5] considered convection in the mushy zone only. Simulations of multicomponent alloys with thermosolutal convection in both the liquid and the mushy zone started appearing in 1995 [6–10]. Modeling multicomponent alloys requires a different algorithmic strategy than those used in earlier studies of binary alloys [11–15], in which knowledge of the temperature in the mushy zone automatically provides the concentration in the interdendritic liquid. In a multicomponent alloy, many combinations of the liquid concentrations can have the same liquidus temperature, making it more difficult to calculate the solidification path.

In numerical calculations, selecting an appropriate mesh spacing is certainly an important step to achieve an accurate simulation. However, none of the aforementioned studies describe, in detail, the method of mesh selection. In 1991, Felicelli [16] recommended that the mesh spacing should be comparable with the solute–decay length scale, D/V, at the dendrite tips, where D is the diffusion coefficient of the solute in the liquid and V is the growth rate. When V is approximately 20 $\mu m\, s^{-1}$ or less, such a spacing is reasonably large enough to achieve a solution that is not prohibitively expensive. With larger growth rates, the mesh spacing based on this criterion is so small that the computations become excessively expensive. Fortunately, the tendency for channels to form exists only when the growth rate is small [7,14], so the criterion D/V is reasonable. When channels do not develop (larger values of V), then mesh spacings greater than D/V (but generally not greater than 1 mm) are adequate.

In past studies [7,10,11,14], the usual method of refining the mesh until calculated results did not change, or at least the extent of segregation did not change, was adopted. In this paper, the sensitivity of mesh spacing on the freckle formation is systematically studied and reported. Based upon the analysis, proper mesh spacing to achieve good accuracy in finite element calculations is recommended to allow one to avoid the expensive trial-and-error procedure of

repetitive calculations with different mesh spacings. As a test alloy, the commercial alloy René N5 is selected; it is one of the second-generation SC superalloys that show excellent creep resistance at high temperatures. From the two-dimensional calculations of rectangular castings, the simulation of macrosegregation and formation of channels/freckles is studied for different solidification conditions and various mesh spacings.

2. MODEL OF SOLIDIFICATION

The transport phenomena and macrosegregation in directional solidification are modeled by a mathematical formulation comprising the energy equation, the momentum equation, and the solute conservation equation. The model for solidification of multicomponent alloys is an extension of a model used in simulations of binary alloys in References [7,8,10,11]. The following simplifying assumptions are made in the governing equations:

1. only solid and liquid phases are present, i.e., no pores form;
2. the flow is Newtonian, laminar, and two-dimensional;
3. the solid and liquid phases have equal and constant physical properties, except in the body force term of the momentum equation;
4. the Boussinesq approximation is made in the buoyancy term of the momentum equation;
5. there is no diffusion of solute in the solid phase; and
6. the solid phase is stationary.

With these assumptions, the equations governing the fluid flow and heat and mass transport are

Continuity:

$$\nabla \cdot \mathbf{u} = 0 \tag{1}$$

Momentum:

$$\phi \frac{\partial}{\partial t}\left(\frac{\mathbf{u}}{\phi}\right) + \mathbf{u} \cdot \nabla\left(\frac{\mathbf{u}}{\phi}\right) = -\frac{\phi}{\rho_0}\nabla p + \frac{\mu}{\rho_0}\nabla^2 \mathbf{u} - \frac{\mu}{\rho_0}\frac{\phi}{\mathbf{K}}\mathbf{u} + \frac{\rho\phi}{\rho_0}\mathbf{g} \tag{2}$$

$$\rho = \rho_0\left[1 + \beta_{\mathrm{T}}(T - T_{\mathrm{R}}) + \sum_{j=1}^{N} \beta_{\mathrm{C}}^{j}(C_{\mathrm{l}}^{j} - C_{\mathrm{R}}^{j})\right] \tag{3}$$

where

$$\beta_{\mathrm{T}} = \frac{1}{\rho_0}\frac{\partial \rho}{\partial T} \tag{4}$$

$$\beta_{\mathrm{C}}^{j} = \frac{1}{\rho_0}\frac{\partial \rho}{\partial C_{\mathrm{l}}^{j}} \tag{5}$$

Energy:

$$\frac{\partial T}{\partial t} + \mathbf{u}\cdot\nabla T = \alpha\nabla^2 T - \frac{L}{c}\frac{\partial \phi}{\partial t} \tag{6}$$

Conservation of solute components:

$$\frac{\partial \bar{C}^j}{\partial t} + \mathbf{u}\cdot\nabla C_l^j = \nabla\cdot(D^j \phi \nabla C_l^j) \tag{7}$$

where

$$\bar{C}^j = \phi C_l^j + (1-\phi)\bar{C}_s^j \tag{8}$$

$$\bar{C}_s^j = \frac{1}{1-\phi}\int_{\phi}^{1} k^j C_l^j \, \mathrm{d}\phi \tag{9}$$

In these equations, ∇ is the gradient operator; $\mathbf{u}$ is the superficial velocity; ϕ is the volume fraction of liquid; t is the time; p is the pressure; μ is the viscosity; $\mathbf{K}$ is the permeability; ρ is the density of the liquid; ρ_0 is the density of the alloy at the reference temperature, T_R, and the reference composition, C_R^j; β_T is the thermal expansion coefficient; β_C^j is the solutal expansion coefficient of element j; $\mathbf{g}$ is the acceleration of gravity; T is the temperature; α is the thermal diffusivity; L is the latent heat; c is the specific heat; k^j is the equilibrium partition ratio of solute j; $\bar{C}^j$ is the total concentration of element j in the mixture of the liquid and solid phases; $\bar{C}_s^j$ is the average concentration of element j in the solid phase; C_l^j is the concentration of element j in the liquid phase; D^j is the diffusion coefficient of element j in the liquid; and N is the number of elements in the alloy. The thermodynamic and transport properties used in the calculations are given in Tables I and II. The permeability is expressed in the principle directions in terms of the volume fraction of liquid, ϕ, and the primary dendrite arm spacing, d_1 [17,18]. Finally, the model assumes that the liquidus temperature of the alloy in the mushy zone, T_L, is a function of the local composition (no undercooling is allowed)

$$T_L = T_R + \sum_{j=1}^{N} m_L^j (C_l^j - C_R^j) \tag{10}$$

where values of m_L^j and C_R^j are given in Table II.

The equations discussed above were discretized and integrated in time using a finite element algorithm that is described in detail by Felicelli *et al.* [7,26]. The model was implemented using a finite element method with bilinear Lagrangian isoparametric elements. Since the pressure is not needed in the calculations, it was eliminated using a penalty function formulation. The solute conservation equation is solved explicitly, but the energy and momentum equations are solved implicitly, requiring a solver. For the momentum equations we used a direct method based on Gaussian decomposition and skyline storage, while for the energy equation we used a conjugate gradient solver with diagonal preconditioning. In both cases, the convective terms

Table I. Thermodynamic and transport properties for René N5.

Reference density (ρ_0 at T_R)	7256.7 kg m^{-3}	[19]
Latent heat of fusion (L)	2.95×10^{5} J kg^{-1}	*
Average thermal conductivity (κ)	32 J K^{-1} m^{-1} s^{-1}	[20]
Average specific heat (c)	774 J kg^{-1} K^{-1}	[20]
Viscosity (μ)	4.929×10^{-3} N s m^{-2}	[21]
Diffusivity of solutes in liquid (D)	5×10^{-9} m^2 s^{-1}	—
Reference temperature (T_R)	1646 K	[22]
Eutectic temperature (T_E)	1606 K	[22]
Thermal expansion coefficient (β_T)	-1.2754×10^{-4} K^{-1}	[19]
Primary dendrite arm spacing: $d_1 = 1.770\times10^{-3}V^{-0.25}\ G^{-0.5}$ (d_1 is in m, V is in m s^{-1}, and G is in K m^{-1})		[22]
Permeability (m^2):		[17,18]

$$K_x=\begin{cases}1.09\times10^{-3}\phi^{3.32}d_1^2 & \phi<0.65\\ 4.04\times10^{-6}\left(\dfrac{\phi}{1-\phi}\right)^{6.7336}d_1^2 & 0.65\le\phi<0.75\\ \left[-6.49\times10^{-2}+5.43\times10^{-2}\left(\dfrac{\phi}{1-\phi}\right)^{0.25}\right]d_1^2 & 0.75\le\phi<1\end{cases}$$

$$K_y=\begin{cases}3.75\times10^{-4}\phi^{2}d_1^2 & \phi<0.65\\ 2.05\times10^{-7}\left(\dfrac{\phi}{1-\phi}\right)^{10.739}d_1^2 & 0.65\le\phi<0.75\\ 0.074[\log(1-\phi)^{-1}-1.49+2(1-\phi)-0.5(1-\phi)^2]d_1^2 & 0.75\le\phi<1\end{cases}$$

* Source: Mueller BA. Private Communication. Howmet Research Center, Whitehall, MI, 1996.

Table II. Solutal expansion coefficients, slopes of liquidus, and equilibrium partition ratios for René N5.

Element, j	Reference concentration, C_R^j (wt.%)	Solutal expansion coefficient, β_C^j (wt.%$^{-1}$) [19]	Slope of liquidus, m_L^j (K wt.%$^{-1}$) [23,24]	Equilibrium partition ratio, k^j [25]
Ta	6.41	4.5743×10^{-3}	−2.55	0.69
Cr	7.11	-1.5142×10^{-3}	−2.15	0.95
Al	6.25	-2.4284×10^{-2}	−5.35	0.96
Co	7.35	-1.1291×10^{-4}	0.01	1.13
W	4.92	5.2203×10^{-3}	2.45	1.67
Re	2.89	5.4580×10^{-3}	5.45	2.0
Mo	1.42	1.8694×10^{-3}	−25.22	0.8

were treated explicitly to keep the matrices symmetric. A Petrov–Galerkin technique for upwinding, in which the weighting function is perturbed in the convective terms of the transport equations, was used. The equations were solved sequentially, with iterations at each time step to achieve convergence. Convergence was established when

$$\left\| \phi_{i+1}^{n+1} - \phi_{i}^{n+1} \right\| < 10^{-4}$$

and

$$\left\| \bar{C}_{i+1}^{j,n+1} - \bar{C}_{i}^{j,n+1} \right\| < 10^{-4}$$

where the $\bar{C}$ values have been non-dimensionalized and superscript n refers to the time step, and subscript i refers to the iteration.

3. SIMULATIONS OF MACROSEGREGATION DURING SOLIDIFICATION

René N5 alloy is directionally solidified by simulation in a rectangular mold of 10 mm in the horizontal direction and 50 mm in the vertical direction; gravity acts downward. Initially, the mold is filled with an all-liquid alloy of the nominal composition in a stable vertical temperature gradient such that the bottom temperature is slightly above that of the liquidus temperature, T_R, and a constant thermal gradient, G, is imposed at the top. A constant cooling rate, r, is applied at the bottom of the mold, and at $t = 0$, small random perturbations (± 0.0005 per cent of the initial concentrations) are introduced in each solute concentration field in order to excite the convection. The full set of boundary and initial conditions is shown in Figure 1.

To predict the macrosegregation, a systematic study of freckle formation as a function of cooling rate was carried out. The initial temperature gradient was held constant at the top ($G = 4000$ K m^{-1}), and the cooling rate at the bottom was varied as $r = 0.16$, 0.20, 0.22, 0.24, 0.28, and 0.32 K s^{-1}. With these cooling conditions, the solidification proceeded with growth rates of approximately 0.026, 0.029, 0.032, 0.034, 0.038, and 0.042 mm s^{-1} respectively, which span cases with freckling to cases with no freckling. At each cooling rate, the computational domain was discretized with uniform meshes of various mesh spacings; a total of 88 simulations were run. All simulations were carried out up to 1200 s of solidification, and resulting macrosegregation of rhenium was plotted. Rhenium (Re) was selected as the element to track because its equilibrium partition ratio deviates the most from unity. Since the partition ratio of Re is greater than one (Table II), it partitions to the solid during solidification, and the concentration of Re in channels/freckles is less than its nominal concentration in the alloy.

Figure 2 shows the typical result with an internal channel/freckle; the applied cooling rate is $r = 0.22$ K s^{-1}, and the finite element mesh comprises square elements in a 40×200 mesh. Figure 2(a) shows the velocity vectors and the contour lines of fraction liquid, and Figure 2(b) shows shaded contour plots of the mixture concentration of Re. Figure 3 shows the case without a channel or freckle and hardly any segregation; the applied cooling rate was increased to $r = 0.28$ K s^{-1}, and the same mesh (40×200) was used. With an increase of the cooling rate, the segregation switches from a freckling case to no freckling case.

Figures 2 and 3 were generated with a finite element mesh comprising square elements. As is shown below, the finite element mesh selected for Figures 2 and 3 was sufficiently refined to accurately predict the macrosegregation in these two cases. Not knowing *a priori* that a mesh is sufficiently refined, however, prevents one from accepting results as being accurate unless

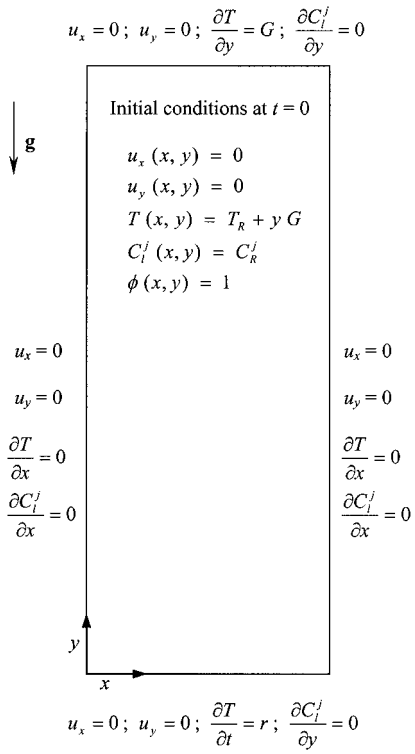

Figure 1. Rectangular domain of mold showing initial and boundary conditions (u_x and u_y are the velocity components in x- and y-directions respectively).

several runs with different mesh spacings are made. Furthermore, since the strengths of convection in the overlying liquid and within the porous mushy zone are very different, one may wish to employ rectangular elements of different sizes along the y-direction, to possibly reduce the number of elements in the domain while still achieving an accurate calculation.

4. RESULTS AND DISCUSSION

To obtain the proper size of elements within the mesh, the sensitivity of mesh size on the macrosegregation was performed. Many cases with combinations of mesh spacings in the range 0.1–1 mm in the x- and y-directions were carried out; these results are summarized in Figure 4. In each graph, the dimensional and non-dimensional mesh spacings in the x- and y-directions are shown, and the area of each bubble shows the degree of segregation as the difference between the minimum mixture concentration and initial concentration of Re. Although the intent is to quantify the degree of segregation by the area of a bubble,

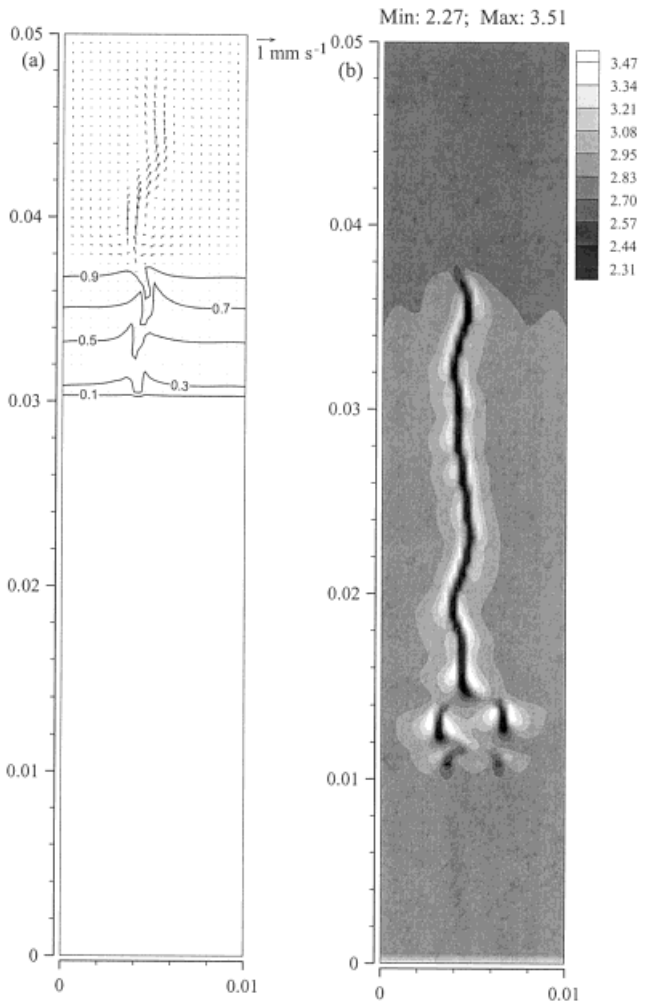

Figure 2. Thermosolutal convection and macrosegregation of Re at 1200 s with $G = 4000$ K m^{-1} and $r = 0.22$ K s^{-1}. (a) Velocity vectors and contour lines of fraction liquid; (b) distribution of total concentration of Re (wt.%). Dimensions are in meters.

coincidentally the smallest bubbles also indicate simulated cases without channels/freckles formation and all of the larger bubbles are simulated cases with channels/freckles. For the latter, the relative per cent deviations of minimum concentrations from the initial concentration of Re are greater than 7 per cent. The sizes of the elements for the bubbles plotted in Figure 4 are also represented non-dimensionally with d_1 and D/V, as characteristic lengths in the x- and y-directions respectively, where d_1 is the primary dendrite arm spacing, D is the diffusion coefficient in the liquid, and V is the growth rate.

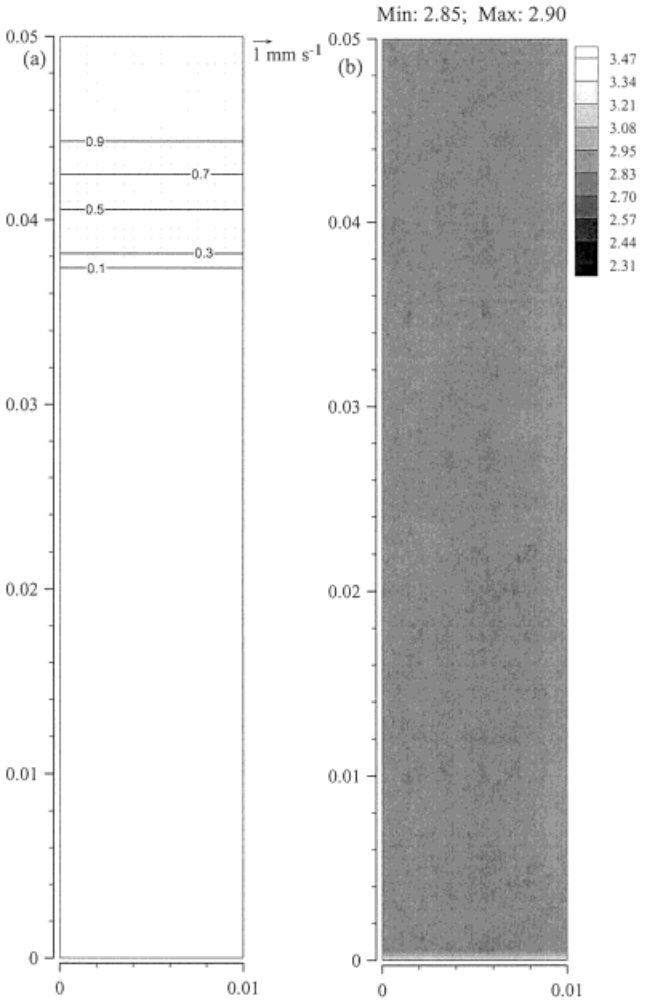

Figure 3. Thermosolutal convection and macrosegregation of Re at 1200 s with $G = 4000$ K m^{-1} and $r = 0.28$ K s^{-1}. (a) Velocity vectors and contour lines of fraction liquid; (b) distribution of total concentration of Re (wt.%). Dimensions are in meters.

Consideration was also given to making Richardson plots of the degree of segregation of Re to access the accuracy of the solutions. In this case, however, the solutions are chaotic, i.e., they are non-periodic solutions, which depend on the perturbations which in turn are affected by the mesh itself. Furthermore, by examination of the longest column of bubbles in each of Figure 4(a)–(f), we see that a log–log plot of the segregation of Re versus the element size in the y-direction does not indicate a rate of convergence.

Figure 4(a) and (b) shows the cases with $r = 0.16$ and 0.20 K s^{-1} respectively. With both cooling rates, all the simulation runs show freckle formation regardless of mesh size. It indicates that, in cases of well-established freckling, the numerical calculation predicts freckling and selection of the mesh size within the scope shown is hardly an issue. However, as the cooling rate increases to $r = 0.22$ K s^{-1} (Figure 4(c)), results are not consistent with all meshes in that if $\Delta x = 1$ mm (about $3d_1$), the simulation falsely indicates no freckling. The situation with $r = 0.24$ K s^{-1} (Figure 4(d)) is more dire, in that when Δy is set at 0.25 mm and $\Delta x \geq 0.33$

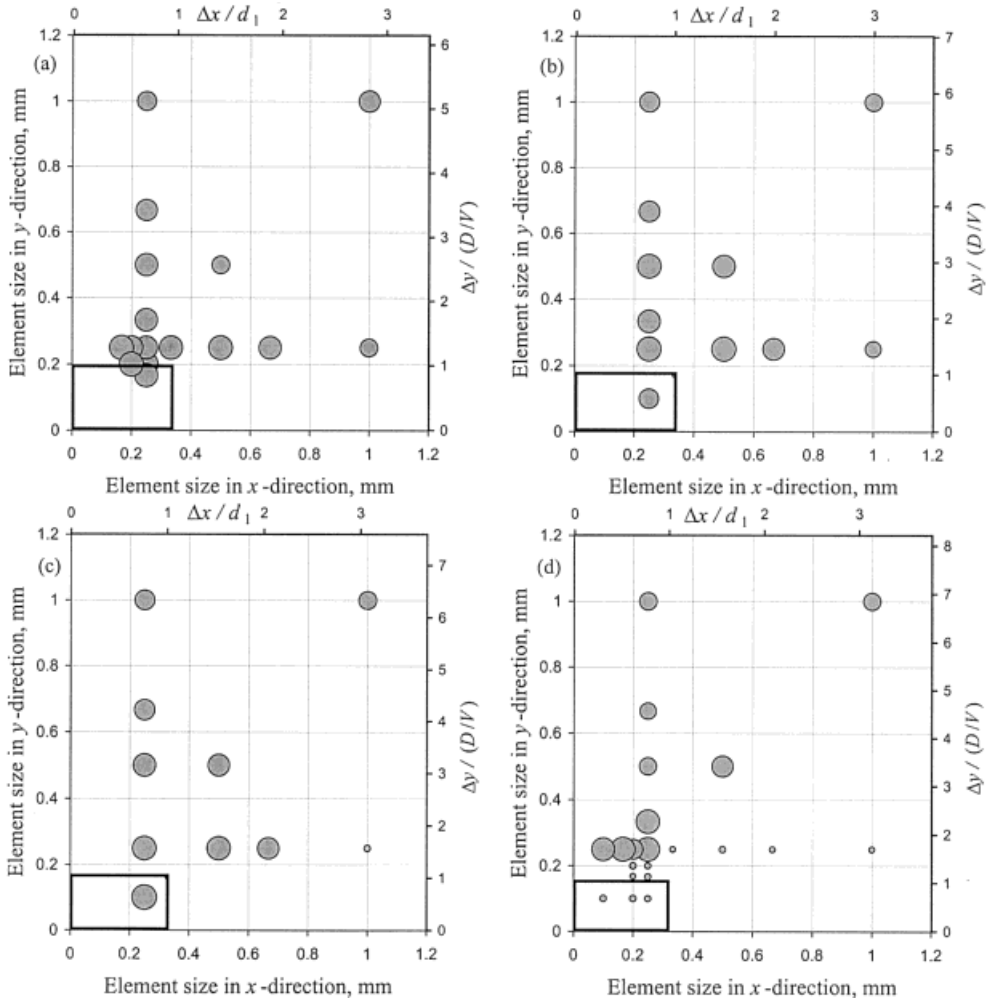

Figure 4. Sensitivity of mesh spacing on simulation results (segregation of Re) with cooling rates of (a) 0.16 K s^{-1}, (b) 0.20 K s^{-1}, (c) 0.22 K s^{-1}, (d) 0.24 K s^{-1}, (e) 0.28 K s^{-1}, and (f) 0.32 K s^{-1}. Bubble size shows amount of segregation; the bold boxes have dimensions of d_1 by D/V.

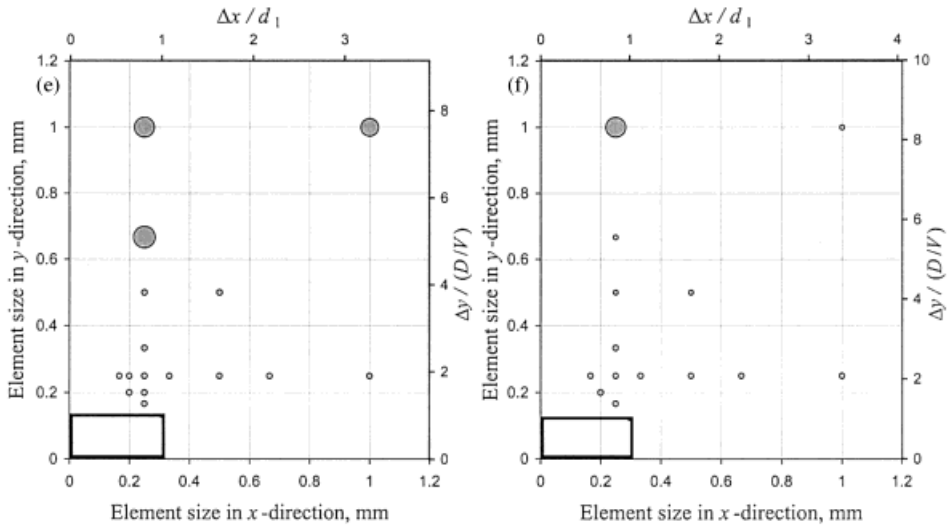

Figure 4 (*Continued*)

mm (about $1.5\,D/V$ and $\geq d_1$ respectively) it appears that there is no freckling, but when $\Delta x \leq 0.25$ mm simulated freckles appear. Hence, one might infer freckling or no freckling depending on the selection of Δx. The most accurate simulations are those closest to the origin, which indicate no freckling.

From the cases with $r = 0.22$–0.32 K s^{-1} (Figure 4(c)–(f)), it is observed that a coarser mesh spacing in the x-direction tends to minimize the simulated macrosegregation. Prediction of the channels/freckles could be missed when the selected mesh spacing in the x-direction is too large. On the other hand, a coarser mesh spacing in the y-direction artificially tends to make the system more unstable. A faulty simulation of channels/freckles can be obtained when the selected mesh spacing in the y-direction is too large.

As it can be seen in the case with $r = 0.32$ K s^{-1} (Figure 4(f)), with one exception the results are not sensitive to the mesh spacing when the cooling rate is high enough for a well-established non-freckling condition. When solidification conditions are close to the limit between freckling and non-freckling (Figure 4(d)), the simulated results are very sensitive to the mesh spacings, especially in the y-direction. Based on the results with the finest mesh spacing, it is deduced that the switching from channels to no channels occurs at $r = 0.24$ K s^{-1}.

Figure 5 is a plot of density of the liquid versus distance through the mushy zone and into the overlying liquid. The solidification conditions are the same as used in generating Figure 4(d) with $\Delta x = 0.1$ mm (about $d_1/3$) and $\Delta y = 0.1$ mm (about $0.7\,D/V$). The density presents a liquid in the mushy zone, which is unstable with respect to convection, but the convection in the mushy zone is diminished because of its low permeability. Most of the liquid in the overlying liquid has a stabilizing density gradient because of the positive thermal gradient. Notice that just above the position of the dendrite tips, there is a layer of small thickness,

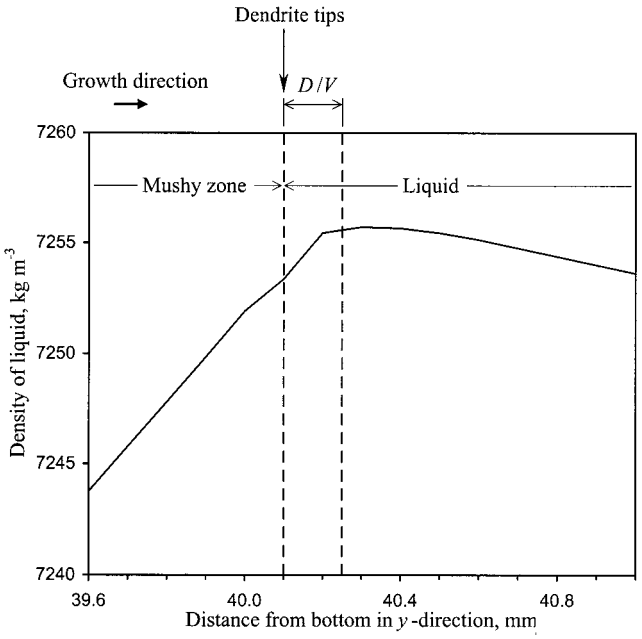

Figure 5. Density of liquid versus distance through mushy zone and into overlying liquid on centerline of casting near dendrite tips at 1200 s of solidification with $G = 4000$ K m^{-1}, $r = 0.24$ K s^{-1}.

which is unstable with respect to the bulk of the overlying liquid. The thickness of this layer is approximately D/V, where D is the diffusion coefficient of the solute in the liquid, and V is the growth rate. Here we have used the same solute diffusivity for all the alloy elements because of a lack of data. When the diffusivities are known for each alloy element, the diffusivity of the slowest diffusing solute should be used. To approximate the growth rate, the average rate to that elevation was calculated. Values of D/V and the primary dendrite arm spacing, d_1, define the bold boxes in Figure 4(a)–(f), with d_1 as the widths and D/V as the heights. These dimensions could be used in all cases as the element dimensions for the finite element mesh in order to achieve accurate simulations, but taking this as a requirement would be unnecessarily stringent. When it is known that the simulation should predict freckling, Figure 4(a)–(c), then the elements can be as large as $2d_1$ by $2\,D/V$. When it is known that freckling should not be predicted by simulation (e.g., Figure 4(e) and (f)), then a considerably coarser mesh of approximately $3d_1$ by $4\,D/V$ can be used. The most troublesome situation is when solidification conditions are very close to the transition between freckling and no freckling. When this happens (Figure 4(d)), then the elements in the uniform mesh should have dimensions no larger than $2d_1$ by $1.5\,D/V$. Since these are the most stringent elements, these dimensions could be selected in any case to accurately predict macrosegregation and whether freckling occurs.

5. CONCLUSIONS

Through a systematic sensitivity analysis of mesh spacing on simulating macrosegregation during directional solidification, the proper mesh spacing in finite element calculations is recommended. The recommended element dimensions of the most stringent case is no larger than $2d_1$ in the x-direction and $1.5\,D/V$ in the y-direction, where d_1 is the primary dendrite arm spacing, D is the diffusivity of the solute in the liquid, and V is the growth rate. With this recommendation, one can avoid the extensive trial-and-error procedure of repetitive calculations with different mesh spacings and consequently save time to attain an accurate prediction from simulations. The size of the elements can be made larger than $2d_1$ by $1.5\,D/V$ when it is known *a priori* that the solidification conditions clearly result in freckling or clearly result in non-freckling.

ACKNOWLEDGMENTS

This work was supported by the Division of International Programs of the National Science Foundation (U.S.A.) and by Consejo Nacional de Investigaciones Científicas y Técnicas (Argentina), under the frame of the international co-operation project 'Simulation of Defects in Castings'. Also, PKS and DRP appreciate the grant provided by National Science Foundation (DMR-9901290), and SDF appreciates the grant provided by Agencia Nacional de Promoción Científica y Tecnológica (PICT98 12-03239).

REFERENCES

1. Beeley PR. Application to aerospace. In *Investment Casting*, Beeley PR, Smart RF (eds). The Institute of Materials: London, 1995; 374–391.
2. Giamei AF, Kear BH. On the nature of freckles in nickel base superalloys. *Metallurgical Transactions* 1970; **1**: 2185–2192.
3. Copley SM, Giamei AF, Johnson SM, Hornbecker MF. The origin of freckles in unidirectionally solidified castings. *Metallurgical Transactions* 1970; **1**: 2193–2204.
4. Flemings MC. *Solidification Processing*. McGraw-Hill: New York, 1974; 244–252.
5. Fujii T, Poirier DR, Flemings MC. Macrosegregation in a multicomponent low alloy steel. *Metallurgical Transactions* 1979; **10B**: 331–339.
6. Schneider MC, Beckermann C. Formation of macrosegregation by multicomponent thermosolutal convection during the solidification of steel. *Metallurgical and Materials Transactions* 1995; **26A**: 2373–2388.
7. Felicelli SD, Poirier DR, Heinrich JC. Macrosegregation patterns in multicomponent Ni-base alloys. *Journal of Crystal Growth* 1997; **177**: 145–161.
8. Felicelli SD, Poirier DR, Giamei AF, Heinrich JC. Simulating convection and macrosegregation in superalloys. *JOM* 1997; **49**: 21–25.
9. Schneider MC, Gu JP, Beckermann C, Boettinger WJ, Kattner UR. Modeling of micro- and macrosegregation and freckle formation in single-crystal nickel-base superalloy directional solidification. *Metallurgical and Materials Transactions* 1997; **28A**: 1517–1531.
10. Felicelli SD, Poirier DR, Heinrich JC. Modeling freckle formation in three dimensions during solidification of multicomponent alloys. *Metallurgical and Materials Transactions* 1998; **29B**: 847–855.
11. Felicelli SD, Heinrich JC, Poirier DR. Simulation of freckles during vertical solidification of binary alloys. *Metallurgical Transactions* 1991; **22B**: 847–859.
12. Bennon WD, Incropera FP. The evolution of macrosegregation in statically cast binary ingots. *Metallurgical Transactions* 1987; **18B**: 611–616.
13. Neilson DG, Incropera FP. Unidirectional solidification of a binary alloy and the effects of induced fluid motion. *International Journal of Heat and Mass Transfer* 1991; **34**: 1717–1732.
14. Poirier DR, Heinrich JC. Simulations of thermosolutal convection in directional solidification. In *Modeling of Casting, Welding and Advanced Solidification Processes VI*, Piwonka TS, Voller V, Katgerman L (eds). The Minerals, Metals, and Materials Society: Warrendale, PA, 1993; 227–234.

15. Beckermann C. Modeling of transport phenomena in mushy zones. In *Modeling of Casting, Welding and Advanced Solidification Processes VI*, Piwonka TS, Voller V, Katgerman L (eds). The Minerals, Metals, and Materials Society: Warrendale, PA, 1993; 181–192.
16. Felicelli SD. Simulation of freckles during vertical solidification of binary alloys. PhD dissertation, The University of Arizona, Tucson, AZ, 1991.
17. Poirier DR. Permeability of flow of interdendritic liquid in columnar-dendritic alloys. *Metallurgical Transactions* 1987; **18B**: 245–255.
18. Bhat MS, Poirier DR, Heinrich JC. Permeability of cross flow through columnar dendritic alloys. *Metallurgical and Materials Transactions* 1995; **26B**: 1049–1056.
19. Sung PK, Poirier DR, McBride E. Estimating densities of liquid transition-metals and Ni-base superalloys. *Materials Science and Engineering* 1997; **A231**: 189–197.
20. Betteridge W, Heslop J (eds). *The Nimonic Alloys and Other Nickel-Base High-Temperature Alloys*. Crane, Russak and Company: New York, 1974; 161–165.
21. McBride E, Poirier DR. Internal report to investment casting cooperative arrangement: materials science based microstructure modeling of multicomponent superalloys. Contract No. MDA972-93-2-0001, The University of Arizona, Tucson, AZ, 1996.
22. Overfelt RA, Matlock C, Sahai V, Matlock D. Microstructure and grain defect formation in directionally solidified René N5. Report to Advanced Research Projects Agency and Investment Casing Cooperative Arrangement, Auburn University, Auburn, AL, 1998.
23. Massalski TB. *Binary Alloy Phase Diagrams* (2nd edn), vols. 1–3. ASM International: Materials Park, OH, 1990; p. 183 (vol. 1); pp. 1215 and 1301 (vol. 2); pp. 2637, 2848, 2867, and 2883 (vol. 3).
24. Nash P. *Phase Diagrams of Binary Nickel Alloys*. ASM International: Materials Park, OH, 1991; pp. 4, 69, 75, 207, 268, 320, and 368.
25. Sung PK, Poirier DR. Liquid–solid partition ratios in nickel-base alloys. *Metallurgical and Materials Transactions* 1999; **30A**: 2173–2181.
26. Felicelli SD, Heinrich JC, Poirier DR. Finite element analysis of directional solidification of multicomponent alloys. *International Journal for Numerical Methods in Fluids* 1998; **27**: 207–227.

